Dynamic Crack-Front Deformations in Cohesive Materials

Thibault Roch, Mathias Lebihain, Jean-François Molinari

Dynamic crack front deformations in cohesive materials

Thibault Roch[1], Mathias Lebihain[2], and Jean-François Molinari[1*]
[1] *Civil Engineering Institute, Materials Science and Engineering Institute, Ecole Polytechnique Fédérale de Lausanne, Station 18, CH-1015 Lausanne, Switzerland*
[2] *Laboratoire Navier, CNRS (UMR 8205), École des Ponts ParisTech, Université Gustave Eiffel, 6-8 avenue Blaise Pascal, 77455 Marne-la-Vallée, France*
(Dated: December 14, 2023)

Crack fronts deform due to heterogeneities, and inspecting these deformations can reveal local variations of material properties, and help predict out-of-plane damage. Current models neglect the influence of a finite dissipation length scale behind the crack tip, called the process zone size. The latter introduces scale effects in the deformation of the crack front, that are mitigated by the dynamics of the crack. We provide and numerically validate a theoretical framework for dynamic crack front deformations in heterogeneous cohesive materials, a key step toward identifying the effective properties of a microstructure.

The propagation of fronts, defining the border between two distinct phases, occurs in numerous physical contexts such as paper wetting [1], combustion [2], polymerization [3] contact mechanics [4], fracture mechanics [5], compressive failure [6] and aseismic slip [7]. Fronts usually roughen due to interaction with heterogeneities. In fracture mechanics, a front marks the spatial separation between intact material and crack, and is thereby called a crack front. It deforms as a consequence of the heterogeneous landscape of toughness, the material resistance to crack propagation. Understanding how these deformations occur allow rationalizing the properties of composite materials [8, 9]. In addition, the transition between faceting and micro-branching for fast crack propagation is thought to be related to high in-plane curvature of the front [10]. Studying the dynamics of front deformations is thus key to unraveling the complex dynamics of heterogeneous dynamic rupture. Coplanar crack propagation is usually studied using perturbative approaches, such as the first-order model derived by Rice [11] based on the weight functions theory of Bueckner [12]. This approach has then been extended to dynamic rupture [13, 14] and also to higher orders [10, 15, 16]. This framework has been successfully applied to the deformation of crack front for various shapes of defects [16–18] as well as predicting the effective toughness of heterogeneous materials [19–21] and rationalizing the intermittent dynamics of crack front propagation in disordered media [22]. These models are however built on the linear elastic fracture mechanics (LEFM) framework and thereby assume that the dissipation at the crack tip occurs in a finite region, the *process zone*, of negligible size. As a consequence, LEFM-based models are bound to treat each asperity scale indifferently. Yet, elasticity is expected to break down along a finite region at the tip of the crack, and heterogeneities smaller or larger than this length scale are expected to affect the crack dynamics differently [23, 24]. Cohesive zone models of fracture [25, 26] allow considering a finite dissipation length scale through the introduction of stresses resisting the crack opening near the tip over a finite length, the process zone size. Regarding crack distortion, a recent theoretical study [27] shed light on the importance of considering the process zone size for quasi-static cracks. The presence of a finite dissipation length scale (i) controls the stability of crack fronts and (ii) introduces scale effects in the pinning of crack fronts by heterogeneities of fracture energy, and these effects are strongly dependent on how the toughness variations are achieved. For dynamic rupture, the process zone size is known to shrink with increasing propagation velocity, thus increasing the importance of this length scale relative to the size of the heterogeneities [28–30]. In this manuscript, we investigate for the first time the influence of a finite process zone on the deformations of a dynamic crack front. We simulate numerically co-planar cracks loaded under normal tensile stress (mode-I) conditions that propagate through a heterogeneous toughness field. We solve this problem using our open-source implementation [31] of the spectral boundary integral formulation of the elastodynamics equations [32, 33] and study the influence of toughness heterogeneities arising from heterogeneities of (i) peak strength and (ii) process zone size. We show that contrarily to LEFM, a finite process zone size introduces scale effects in crack front deformations, related to the nature of the heterogeneities. We also show that dynamic cracks become more and more oblivious to the nature of heterogeneities and their intensity as their speed approaches the Rayleigh wave speed. The behavior of dynamic crack fronts is comprehensively understood with an analytical model that rationalizes the numerical front deformations.

We consider two semi-infinite elastic bodies of section L_x, L_z that are in contact along a planar interface at $y = 0$ (see Fig. 1a). Periodic boundary conditions are imposed in the x and z directions. The bodies are loaded under mode-I condition that drives a cohesive crack through a planar interface (crack in brown, process zone in orange in Fig. 1b) in the positive x direction at a constant velocity v_c. The propagation in the $-x$ direction is prevented. The crack initially propagates in-

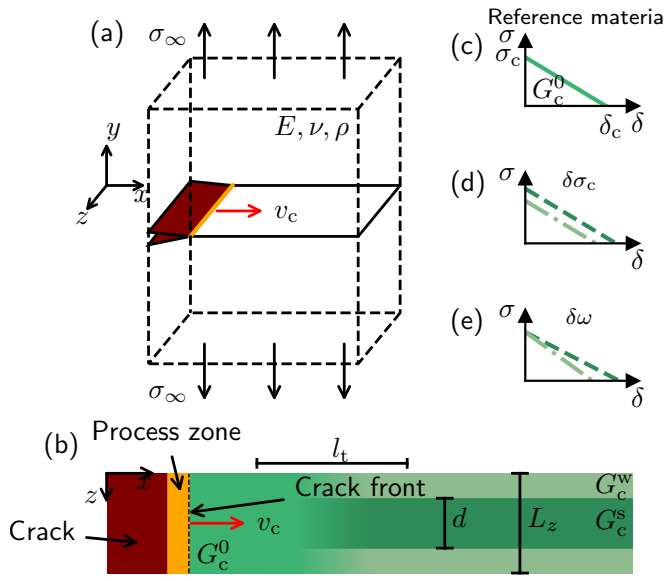

FIG. 1. (a) Two identical semi-infinite elastic bodies are in contact at a planar interface located at $y = 0$, and are loaded under normal tensile stress that drives a crack at a constant velocity v_c. (b) The layout of the interface with the crack (brown), the process zone (orange), and the toughness field (shades of green). The crack front (dashed black line) marks the separation between the process zone and the intact material. (c) Traction-separation law for the reference material. Toughness heterogeneities are achieved by (d) changing the peak strength σ_c or (e) changing the quasi-static process zone size ω_0 but keeping the peak strength constant.

side a homogeneous field of reference toughness G_c^0. The interface properties are then gradually changed along a distance l_t towards an x invariant field composed of a stripe of larger toughness G_c^s (dark green) of width d embedded in a weaker toughness field G_c^w (light green). The average toughness in the z direction is kept equal to the reference one, $(G_c^s + G_c^w)/2 = G_c^0$, resulting in an effective toughness in the weak pinning regime (the crack front maintains a stationary shape while propagating) that is equal to G_c^0 [27]. The gradual transition of properties allows reducing the oscillations of the crack front deformations, see [34]. In this manuscript, we use $d = L_z/2$, $L_x = 8L_z$. We study the propagation for only $x < 0.75L_x$ to neglect the effect of periodicity. We employ a linear cohesive law (see Fig. 1c) to describe the behavior of the interface, for which the stress decays linearly from a peak value σ_c to 0 with the opening δ up to a critical value δ_c

$$\sigma^{str}(x, z, t) = \sigma_c(x, z) \max\left[1 - \delta(x, z, t)/\delta_c(x, z), 0\right] \quad (1)$$

For the linear slip weakening law, the process zone size at rest ω_0 can be estimated as $\omega_0 \simeq 0.731(1-\nu)\mu\delta_c/\sigma_c$ [36], with ν and μ the Poisson's ratio and the shear modulus of the bulk. The opening is defined as the difference between the displacement fields of the top and bottom solids. In this work, we investigate two types of heterogeneities: (1) heterogeneities of peak strength σ_c with equal process zone size (see Fig. 1d) or (2) heterogeneities of quasi-static process zone size ω_0 with constant peak strength (see Fig. 1e). The toughness contrast is defined as $\Delta G_c = G_c^s - G_c^w$. The problem is solved by conducting full-field dynamic calculations, using an in-house open-source implementation of the spectral boundary integral method [32, 33, 37] called cRacklet [31]. The details of the method are available in [34]. The crack front is initially perfectly straight and starts deforming when it reaches the heterogeneous field of toughness. The dynamic deformation of the crack front is mediated by the propagation of crack front waves [29, 38, 39], resulting in the front oscillating over an equilibrium configuration, see [34] . We measure the amplitude A of the front deformations as the distance between the most advanced point in the process zone at the axis of the strong band and at the axis of the weak band, see Fig. 2b. We started by validating the ability of our numerical model to capture the linear increase of front deformations amplitude with the toughness contrast, see [34].

First, we investigate the effect of the propagation velocity on the dynamic crack front deformations. The process zone size at rest ω_0 is kept relatively small compared to the heterogeneities size, and the contrast in toughness is achieved by varying the peak strength while keeping the process zone size at rest constant across the interface. According to [40], a front dynamically stiffens with increasing propagation velocity and thus diminishes its deformations. For fast cracks, more energy is stored as kinetic energy resulting in comparatively lower stored elastic energy and consequently less front deformations. We show in Fig. 2a the amplitude A of front deformations as a function of the propagation velocity with $v_c/c_R \in [0.3 - 0.9]$ (black diamonds), with c_R the Rayleigh wave speed. The amplitude indeed decreases for faster cracks. The effect of dynamic stiffening on front deformations can be quantified by the function $D_I(v_c)$ which only depends on the propagation velocity and whose derivation is given in [34]. The dashed black line in Fig. 2a is $D_I(v_c)A_{\text{lefm}}/d$, with A_{lefm} the predicted amplitude of front deformations based on the classical line tension model which is valid for small process zone size, and this function matches the amplitude observed in the simulations. Fig. 2b-d are snapshots of the crack front configuration for $v_c/c_R = 0.3, 0.6, 0.9$. The crack is shown in brown, the process zone size in orange, and the shades of green stand for the toughness of the intact part of the interface. In these snapshots, two effects of an increasing crack velocity are visible: (i) a decrease in the deformations and (ii) a decrease in the process zone size. The latter is known as the Lorentz contraction [28] of the process zone and is highly relevant for the following when

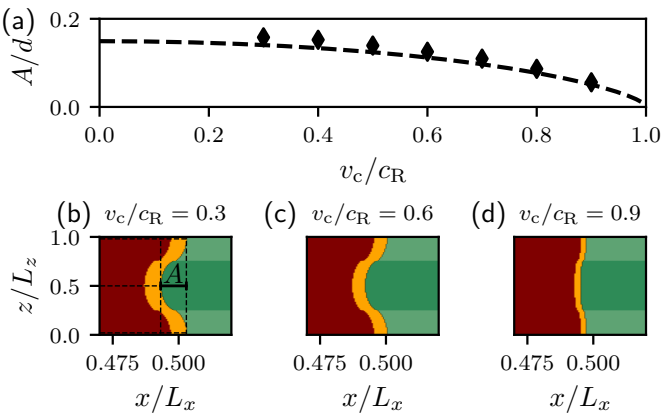

FIG. 2. (a) Normalized amplitude A/d of the front deformations as a function of the normalized propagation velocity v_c/c_R, with the prediction of the classical dynamic line tension model $D_I(v_c)A_{\text{lefm}}/d$ (dashed black), see details in the text. (b)-(c)-(d) Snapshots of the interface (with the crack in brown, the process zone in orange, and the intact interface in shades of green corresponding to the toughness) for respectively $v_c/c_R = 0.3, 0.6, 0.9$ and $\Delta G_c/G_c^0 = 0.4$. Note that the x-scale and z-scale are different.

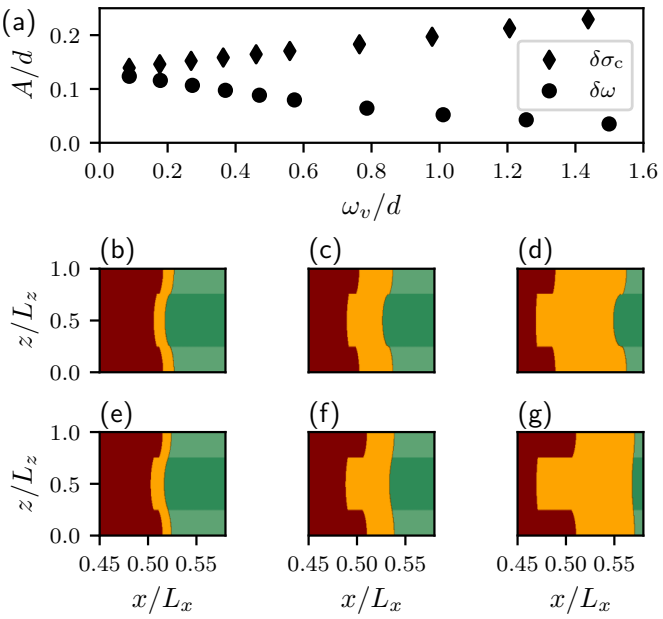

FIG. 3. (a) Scaling of the amplitude A of the front deformations with the process zone size ω_v for heterogeneities of constant process zone size (diamonds, snapshots in (b)-(c)-(d) for $\omega_v/d \sim 0.2, 0.6, 1.25$) and constant peak strength (circles, snapshots in (e)-(f)-(g) for $\omega_v/d \sim 0.2, 0.6, 1.25$). For the latter, ω_v is the average of $\omega_v(z)$ over the crack front. For these simulations $v_c = 0.5c_R$ and $\Delta G_c/G_c^0 = 0.4$.

we assess the effect of this length scale on front deformation. The instantaneous process zone size for a mode I crack is given by $\omega_v = \omega_0/A_I(v_c)$ with A_I a universal function of the crack velocity [41].

The influence of the process zone size is investigated. We consider two cases: heterogeneities of peak strength σ_c (with constant process zone, see Fig 1d), and heterogeneities of process zone size at rest ω_0 with constant peak strength, see Fig 1e). We vary in both cases the average value ω_0 of the quasi-static process zone size while keeping the toughness contrast and the propagation velocity constant. The amplitude of front deformations is shown in Fig. 3a, for $v_c = 0.5c_R$, $\Delta G_c = 0.4G_c^0$ and $\omega_v/d \in [0.05 - 1.5]$ for both heterogeneities of peak strength (diamonds) and process zone size (circles). For small relative process zone size ω_v/d the amplitude is similar for both types of heterogeneities. However, they get significantly farther apart with increasing process zone size: it increases with the dissipation length scale for heterogeneities of peak strength, while it diminishes for heterogeneities of process zone size. Note that this behavior is qualitatively generic and does not depend on the propagation velocity v_c. Changes in process zone size are accommodated more easily by a crack front than changes in peak strength. These observations are striking: the deformations of a cohesive crack propagating through a heterogeneous microstructure are strongly dominated by the nature of the heterogeneities. For two interfaces sharing the same fracture toughness contrast, the difference between the two types of heterogeneities investigated in this work reaches up to a factor 4 when the process zone and the heterogeneities have the same size $\omega_v/d \sim 1$. The deformations are not tied directly to the toughness contrast, but rather to the variations of the cohesive parameters. For the slip-weakening law used in this manuscript and heterogeneities achieved by varying both the peak strength and the process zone size (not presented here), we expect the behavior to be bounded by the two limiting cases that were investigated. This difference vanishes for negligibly small relative process zone size, which can occur either with brittle materials or when cracks propagate at a velocity close to the limiting wave speed due to the Lorentz contraction.

In order to understand these surprising observations, we go back to the *quasi-static cohesive line tension model* that has been recently derived in [27]. Two competing mechanisms arise from the presence of a cohesive zone : (i) the front is *looser* at scales comparable to that of the spatially localized micro-damage, (ii) the fluctuations of strength $\delta\sigma_c$ and process zone $\delta\omega$ at that scale are also smoothed out. These competing effects can have two different outcomes in the quasi-static regime [27] that can be understood with the fluctuations of cohesive stress that give rise to a stress intensity factor. The influence of their spatial distribution is controlled by the length scales of the front deformation (d and A). Disorder of strength results in fluctuations concentrated near the tip, so that the front has to distort more to conform to the disordered landscape (increase of A). For heterogeneities of process

zone, the fluctuations occur throughout the entire process zone and especially in its wake, such that the front does not distort much (decrease of A). The overall size of the process zone size ω_v impact the intensity of the cohesive stress fluctuations, thus ruling the potency of these effects on A. This is in qualitative agreement with the results reported in Fig. 3a. However, our simulations correspond to fully dynamic rupture while [27]'s model is limited to quasi-static cracks. Two additional effects are expected to emerge when extending this model to dynamics: (iii) the process zone size changes dynamically and shrinks when a crack accelerates due to the Lorentz contraction [28] and (iv) the front stiffens with increasing crack velocity [40]. For the same interface, a faster crack is expected to deform less, and the differences between the type of heterogeneities should be reduced. In order to validate our observations, we extend the model of [27] to dynamics in steady state (i.e., constant propagation velocity, see details in [34]) and obtain for the front deformations δa :

$$\frac{\widehat{\delta a}(k)}{\omega_v} = -D_I(v_c)\left(\frac{\hat{\Sigma}(|k|\omega_v)}{\hat{\mathcal{A}}(|k|\omega_v)}\frac{\widehat{\delta\sigma_c}(k)}{\sigma_c^0} + \frac{\hat{\Omega}(|k|\omega_v)}{\hat{\mathcal{A}}(|k|\omega_v)}\frac{\widehat{\delta\omega}(k)}{2\omega_v}\right) \tag{2}$$

with k the wavenumber, $\hat{\cdot}$ indicating a Fourier transform, ω_v the instantaneous process zone size (related to (iii) above), and $D_I(v_c)$ a function of the velocity that represents the dynamic stiffening of the front (point (iv) above). $\hat{\mathcal{A}}$, $\hat{\Sigma}$, and $\hat{\Omega}$ are functions of the nature of the weakening, the wavenumber, and the process zone size (see [34] for their formulation). $\hat{\mathcal{A}}$ acts as (i) the *loss of stiffness* of the front due to the introduction of a finite-size region of dissipation, while $\hat{\Sigma}$ and $\hat{\Omega}$ (ii) smooth out the fluctuations of material properties. In the limit of small ω_v/d, the classical line tension model is recovered.

Crack front deformation simulations have been conducted for a broad range of parameters, including variations of process zone size at rest ω_0, toughness contrast, heterogeneity type, and front velocity v_c. In Fig. 4a the amplitudes measured from the simulations are compared to the predictions from the classical line tension model (i.e., not considering the influence of the process zone size), with the dynamic stiffening term (from Eq. S8). This prediction fails, as we have established previously that a finite process zone size strongly impacts the front deformations. For a given prediction based on LEFM (take for example $A_{\mathrm{lefm}}/d = 0.25$) there is a large spread of measured amplitude, being either larger or lower than the predicted one (the dashed-gray line has a slope of 1) depending on the heterogeneity type. It is expected from the observations of Fig. 3 that simulations with a small process zone (e.g., for fast ruptures) will result in a significantly smaller difference between the two types of heterogeneities. This is apparent with the data points corresponding to fast cracks (yellow-green in Fig. 4a) that

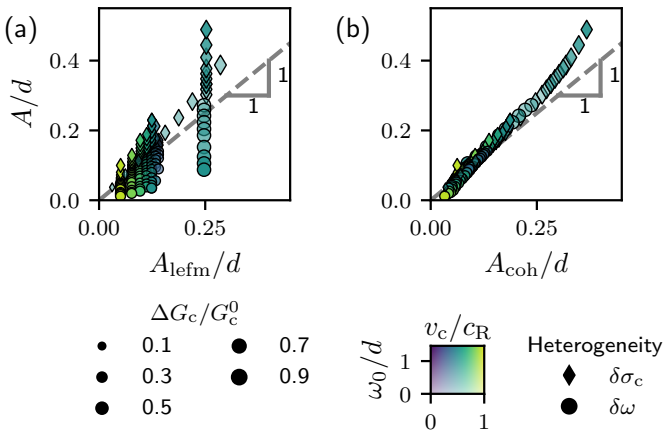

FIG. 4. The front deformations amplitude measured in simulations versus (a) the LEFM prediction not accounting for a finite process zone, (b) the prediction from our newly derived *dynamic cohesive line tension model*. v_c, ω_0, ΔG_c, and the type of heterogeneities have been systematically varied (the detailed description of each data point is available in [34]).

are significantly closer than the ones for slower cracks (in blue). The effect of the front stiffening is also visible from Fig. 4a, with large velocities resulting in small amplitudes. In Fig. 4b, the prediction of Eq.(2), the newly derived *dynamic cohesive line tension model*, is tested: all the data fall close to a linear master curve, strongly supporting the validity of our model for rationalizing the effect of a finite process zone. While the predictions of Eq. (2) are based on the assumption of a semi-infinite crack, finite-size cracks have been considered in the simulations. Plus, the simulated ruptures are not in a steady-state as assumed in the model. Second-order effects might also be required to accurately describe the deformations of cohesive fronts, as the latter can display larger curvatures than the classical line tension fronts. This could potentially explain the small deviations from the predictions. Nonetheless, the proposed model successfully predicts the numerical observations and thereby the non-trivial influence of a finite dissipation length scale for crack front deformations at constant propagation velocity: not only does the process zone influence front deformations, but also its outcome varies strongly depending on heterogeneity type.

The deformations of a dynamic cohesive crack propagating through a heterogeneous field of toughness have been investigated numerically using the spectral boundary integral method coupled with a cohesive zone model. We show that contrarily to LEFM, a finite process zone size introduces scale effects in the deformation of the crack front that are non-trivial and depend on the nature of the heterogeneities. Fast cracks become more and more oblivious to (i) the nature of the disorder due to the Lorentz contraction of the process zone, and (ii) its intensity due to the dynamic stiffening of the front. To

rationalize these observations, we extended the *cohesive line tension model* recently proposed in [27] to dynamic rupture. This model allows considering heterogeneities at multiple scales, from the nanoscale up to the mesoscale, and predicts accurately the amplitude of the observed deformations, taking into account the instantaneous average process zone size and the propagation velocity. All in all, our model reveals the non-trivial effect of a finite dissipation length scale on the front deformations and particularly the importance of the nature of the heterogeneities. Building a complete cohesive model including changes in velocity and variations of properties along the front propagation direction remains a challenge. For the latter, the process zone size is expected to be also the relevant length scale, as the properties are averaged over the process zone size [23].

We focused here on steady-state crack propagation when material disorder is invariant in the propagation direction. In this limit case, called weak pinning regime, the energy dissipated in fracture is proportional to the average fracture energy G_c^0. As soon as the translational invariance breaks, crack propagation articulates as the succession of depinning instabilities, and an additional toughening arises from the disorder [42]. The instability threshold is controlled by the energy landscape experienced by the rough crack front. While we do not quantify here the energy balance of dynamic cohesive ruptures, our model provides the necessary ingredients to characterize the impact of the process zone size and heterogeneities on the front roughness, and so on the effective toughness. However, one can already foresee that nearly Rayleigh-wave-speed co-planar cracks with dynamically straightened fronts should propagate in the weak pinning regime. Finally, this work might help understand the occurrence of out-of-plane damage as a consequence of high in-plane curvature of the front [10], and more generally the deformations of a three-dimensional crack front for which the process zone size changes with the orientation from the crack tip.

* jean-francois.molinari@epfl.ch

[1] A. S. Balankin, R. G. Paredes, O. Susarrey, D. Morales, and F. C. Vacio, Phys. Rev. Lett. **96**, 056101 (2006).
[2] J. Maunuksela, M. Myllys, O.-P. Kähkönen, J. Timonen, N. Provatas, M. J. Alava, and T. Ala-Nissila, Phys. Rev. Lett. **79**, 1515 (1997).
[3] E. M. Lloyd, E. C. Feinberg, Y. Gao, S. R. Peterson, B. Soman, J. Hemmer, L. M. Dean, Q. Wu, P. H. Geubelle, N. R. Sottos, and J. S. Moore, ACS Cent. Sci. **7**, 603 (2021).
[4] A. Sanner and L. Pastewka, Journal of the Mechanics and Physics of Solids **160**, 104781 (2022).
[5] J. Schmittbuhl and K. J. Maloy, Phys. Rev. Lett. **78**, 3888 (1997).
[6] E. Berthier, A. Mayya, and L. Ponson, Journal of the Mechanics and Physics of Solids **162**, 104826 (2022).
[7] A. Sáez, B. Lecampion, P. Bhattacharya, and R. C. Viesca, Journal of the Mechanics and Physics of Solids **160**, 104754 (2022).
[8] V. Lazarus, J. Mech. Phys. Solids **59**, 121 (2011).
[9] D. Bonamy and E. Bouchaud, Phys. Rep. **498**, 1 (2011).
[10] I. Kolvin, J. Fineberg, and M. Adda-Bedia, Phys. Rev. Lett. **119**, 215505 (2017).
[11] J. Rice, J. Appl. Mech. **52**, 571 (1985).
[12] H. Bueckner, Int. J. Solids Struct. **23**, 57 (1987).
[13] J. R. Willis and A. B. Movchan, J. Mech. Phys. Solids **43**, 319 (1995).
[14] A. B. Movchan and J. R. Willis, J. Mech. Phys. Solids **43**, 1369 (1995).
[15] J.-B. Leblond, S. Patinet, J. Frelat, and V. Lazarus, Eng. Fract. Mech. **90**, 129 (2012).
[16] M. Vasoya, J.-B. Leblond, and L. Ponson, Int. J. Solids Struct. **50**, 371 (2013).
[17] J. Chopin, A. Prevost, A. Boudaoud, and M. Adda-Bedia, Phys. Rev. Lett. **107**, 144301 (2011).
[18] S. Xia, L. Ponson, G. Ravichandran, and K. Bhattacharya, Phys. Rev. Lett. **108**, 196101 (2012).
[19] S. Patinet, D. Vandembroucq, and S. Roux, Phys. Rev. Lett. **110**, 165507 (2013).
[20] S. M. Xia, L. Ponson, G. Ravichandran, and K. Bhattacharya, J. Mech. Phys. Solids **83**, 88 (2015).
[21] M. Lebihain, Int. J. Fract. **230**, 99 (2021).
[22] J. Barés, A. Dubois, L. Hattali, D. Dalmas, and D. Bonamy, Nat. Comm. **9**, 1253 (2018).
[23] F. Barras, P. H. Geubelle, and J.-F. Molinari, Physical Review Letters **119**, 144101 (2017).
[24] D. S. Kammer, D. Pino Muñoz, and J. F. Molinari, J. Mech. Phys. Solids **88**, 23 (2016).
[25] D. S. Dugdale, J. Mech. Phys. Solids **8**, 100 (1960).
[26] G. I. Barenblatt, in *Adv. Appl. Mech.*, Vol. 7, edited by H. L. Dryden, T. von Kármán, G. Kuerti, F. H. van den Dungen, and L. Howarth (Elsevier, 1962) pp. 55–129.
[27] M. Lebihain, T. Roch, and J.-F. Molinari, J. Mech. Phys. Solids **168**, 105025 (2022).
[28] J. R. Rice, in *in Physics of the Earth's Interior, edited by A.M. Dziewonski and E. Boschi* (1980) pp. 555–649.
[29] J. W. Morrissey and J. R. Rice, J. Mech. Phys. Solids **46**, 467 (1998).
[30] I. Svetlizky and J. Fineberg, Nature **509**, 205 (2014).
[31] T. Roch, F. Barras, P. H. Geubelle, and J.-F. Molinari, J. Open Source Softw. **7**, 3724 (2022).
[32] P. H. Geubelle and J. R. Rice, J. Mech. Phys. Solids **43**, 1791 (1995).
[33] M. S. Breitenfeld and P. H. Geubelle, Int. J. Fract. **93**, 13 (1998).
[34] See supplemental material at [url will be inserted by publisher] for additional details on the material properties, the numerical scheme, the identification of the equilibrium amplitude in the simulations and the derivation of the dynamic cohesive line tension model, which includes ref.
[35] S. Ramanathan and D. S. Fisher, Phys. Rev. Lett. **79**, 877 (1997).
[36] R. C. Viesca and D. I. Garagash, J. Mech. Phys. Solids **113**, 13 (2018).
[37] J. W. Morrissey and P. H. Geubelle, Int. J. Numer. Methods Eng. **40**, 1181 (1997).
[38] F. Fekak, F. Barras, A. Dubois, D. Spielmann, D. Bonamy, P. H. Geubelle, and J. F. Molinari, J. Mech.

Phys. Solids **135**, 103806 (2020).
[39] A. Dubois and D. Bonamy, Phys. Rev. E **103**, 013004 (2021).
[40] J. W. Morrissey and J. R. Rice, J. Mech. Phys. Solids **48**, 1229 (2000).
[41] L. B. Freund, *Dynamic Fracture Mechanics* (Cambridge university press, Cambridge, 1998).
[42] V. Démery, A. Rosso, and L. Ponson, Europhys. Lett. **105**, 34003 (2014).

Supplemental Material for Dynamic crack-front deformations in cohesive materials

Spectral Boundary Integral Method

The simulations are performed using an in-house open-source implementation (called cRacklet [1]) of the spectral boundary integral formulation of the elastodynamic equations [2–4]. This method describes the behavior at the interface between two semi-infinite elastic solids. The basic relation between the interfacial stresses $\boldsymbol{\sigma}$ and the opening displacements $\boldsymbol{u}^{\pm}$ in this case is given in Eq. (S1):

$$\boldsymbol{\sigma}(\boldsymbol{x},t)^{\pm} = \boldsymbol{\sigma}^{\pm}_{\boldsymbol{\infty}}(t) - \underline{\boldsymbol{V}}\frac{\partial \boldsymbol{u}^{\pm}}{\partial t} + \boldsymbol{s}^{\pm}(\boldsymbol{x},t) \tag{S1}$$

The $+$ and $-$ superscripts stand for the top and bottom solid. The first contribution is the remotely applied loading $\boldsymbol{\sigma_\infty}(t)$, the second is the so-called radiation damping term where $\underline{\boldsymbol{V}}$ is a diagonal matrix with

$$V_{xx} = V_{zz} = \mu/c_{\mathrm{s}}, V_{yy} = \mu c_{\mathrm{d}}/c_{\mathrm{s}}^2 \tag{S2}$$

μ the shear modulus, c_{s} and c_{d} respectively the shear wave speed and the longitudinal wave speed. $\boldsymbol{s}(x,t)$ represents the spatio-temporal interaction of different points on the interface mediated by bulk elastodynamics and is related to the interfacial displacement history through a convolution integral. Its Fourier representation can be found in [4]. Eq. (S1) is completed by interface conditions (Eq. (1)): as long as the stress at the interface is lower than the interfacial strength, continuity of tractions and displacements are satisfied at the interface. Otherwise, the interface is opening: the velocity is computed such that the stresses are in equilibrium with the strength of the interface given by Eq.(1) as a function of the displacement jump. The displacement $\boldsymbol{u}(\boldsymbol{x},t)$ is then integrated in time using an explicit time-stepping scheme:

$$\boldsymbol{u}(\boldsymbol{x},t+\Delta t) = \boldsymbol{u}(x,t) + \frac{1}{2}\frac{\partial \boldsymbol{u}(x,t)}{\partial t}\Delta t \tag{S3}$$

with the time step being $\Delta t = \alpha \Delta x/c_{\mathrm{s}}$, where Δx is the numerical grid spacing. The numerical parameter α is chosen to ensure the stability and the convergence of the numerical scheme, and is typically set to 0.2. In our numerical simulations, the interface is initially at rest under homogeneous tensile stresses. A crack is slowly grown until it spontaneously propagates at the targeted velocity. The loading is tailored from a reference simulation in a 2D setup with homogeneous interfacial properties such that the crack velocity is constant during propagation.

Material properties

The simulations reported in the manuscript have been conducted using the elastic material properties of Homalite: Young's Modulus $E = 5.3e9$ [Pa], Poisson's ratio $\nu = 0.35$ [-] and shear wave speed $c_{\mathrm{s}} = 1263$ [m/s]. For the interface behavior, the fracture toughness $G_c^0 = 90$ [J/m^2] is defined by a couple of maximum stress and critical opening values between $(\sigma_c^0, \delta_c^0) = (7.79\times 10^6, 2.31\times 10^{-5})$ [Pa,m] and $(\sigma_c^0, \delta_c^0) = (2.08\times 10^6, 8.64\times 10^{-5})$ [Pa,m] . The process zone at rest associated to these parameters goes from $\omega_0 = 6.54\times 10^{-3}$ [m] to $\omega_0 = 9.15\times 10^{-2}$ [m].

For heterogeneities of strength, the strength in the weak and strong bands are defined as:

$$\begin{aligned}\sigma_{\mathrm{c}}^s &= \sigma^0\left(1+\frac{\delta G_{\mathrm{c}}}{2}\right)^{1/2}\\ \sigma_{\mathrm{c}}^w &= \sigma^0\left(1-\frac{\delta G_{\mathrm{c}}}{2}\right)^{1/2}\end{aligned} \tag{S4}$$

For heterogeneities of process zone, the process zone size in the weak and strong bands are defined as :

$$\begin{aligned}\omega_0^s &= \omega_0^0\left(1+\frac{\delta G_{\mathrm{c}}}{2}\right)\\ \omega_0^w &= \omega_0^0\left(1-\frac{\delta G_{\mathrm{c}}}{2}\right)\end{aligned} \tag{S5}$$

The full details of each simulation and the code used to run the simulations are available at [5].

Time evolution of the crack deformations and crack front waves

The deformation of the crack front is not instantaneous. When a crack starts interacting with a heterogeneous field of toughness, the perturbation propagates along the front via crack front waves [6, 7]. If the change in toughness is abrupt, the front deformation amplitude overshoots its final value and then oscillates around it. The amplitude of these oscillations decreases slowly with time $\propto 1/\sqrt{t}$. As we are interested in the value of the equilibrium amplitude, we change progressively the toughness properties along a length l_t to reduce the amplitude of these oscillations, such that the simulated cracks are closer to a permanent regime. We illustrate in Fig. S1 the time evolution of the amplitude of the crack front normalized by the heterogeneity size in two cases: one with an abrupt change of toughness, i.e. $l_{\mathrm{t}} = 0$ (yellow diamonds) and a case with $l_{\mathrm{t}} = 5\omega_v$ (brown circles). For these two simulations, $\Delta G_c/G_c^0 = 0.4$, $v_c/c_r = 0.7$ and $\omega_0/d \sim 0.42$. The oscillations of the front amplitude are significantly reduced when the material properties are slowly changed over the transition length l_{t}. A

longer transition length would diminish the oscillations even more, but would require to enlarge the length of the system and increase the computational cost.

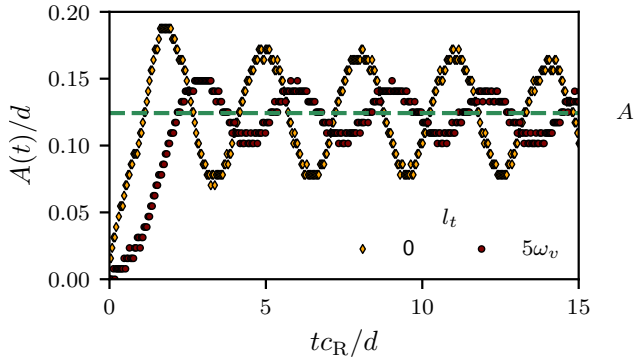

FIG. S1. Evolution of the amplitude of the front deformations as a function of time for two simulations with $v_c = 0.7c_R$, $\Delta G_c/G_c^0 = 0.4$ and $\omega_0/d \simeq 0.42$. The yellow diamonds correspond to an interface with an abrupt change of properties $l_t = 0$. The results corresponding to an interface with a gradual change of properties over the transition length $l_t \simeq 5\omega_v$ are shown with brown circles. The green line indicates the steady-state amplitude around which the instantaneous amplitude oscillates.

The period of oscillations is characteristic of the propagation velocity of the crack front waves: the time interval between two local extrema corresponds to the time that is required for the crack front waves to propagate across a distance d. When possible, we computed the velocity of the crack front waves and reported them in Fig. S2. Note that in some cases the oscillations are almost completely eliminated, and thus it is not possible to easily measure the velocity of the crack front waves. This is mostly the case for simulations with large process zone size. The change of properties in the x direction is averaged over the process zone size, leading to an apparent change in toughness that is smoother and resulting in crack front waves with lower amplitude. The velocities of the crack front wave in our simulations are in agreement with the theoretical prediction given by [8] (in dashed gray in Fig S2). The spread around the theoretical prediction for a given crack velocity is related to the difficulty in computing the crack front wave velocity. Contrarily to the case originally explored by [6] in mode I or later by [7] in mode II, in which a single asperity creates a perturbation whose propagation along the front is clearly visible, the heterogeneous pattern investigated in this manuscript results in the front shape changing at every position along z at the same time, leading to a challenging identification of the front wave velocity. The latter is computed as explained previously by identifying the period of oscillations, and thus requires finding local extrema of a discrete set of points. The procedure used here involves smoothing the data, which might alter slightly the precision of the results.

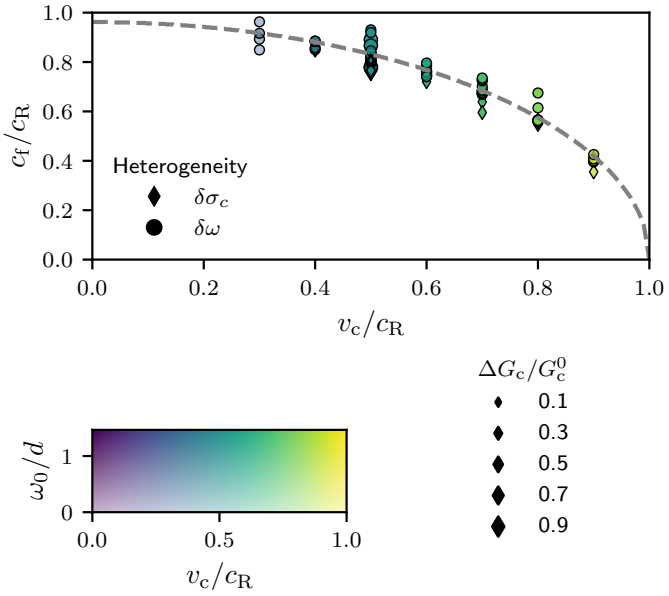

FIG. S2. Crack front wave velocity c_f as a function of the front velocity v_c. The dashed gray line is the theoretical prediction following [8]. Not all the simulations are shown in this figure as it is not always possible to determine the crack front wave velocity properly.

Toughness contrast with constant process zone size

To assess the validity of the numerical model, we first investigate the effect of the toughness contrast on the dynamic crack front deformations. The process zone is kept relatively small compared to the heterogeneities size, and the contrast in toughness is achieved by varying the peak strength while keeping the process zone size constant across the interface. The amplitude of the front deformations, normalized by the heterogeneities size, is shown in Fig. S3a as a function of the toughness contrast for $\Delta G_c/G_c^0 \in [0.1, 1.4]$. Fig. S3b-d are snapshots of the crack front configuration for $\Delta G_c/G_c^0 = 0.3, 0.7, 1.2$. The crack is shown in brown, the process zone size in orange, and the shades of green stand for the toughness of the intact part of the interface. We observed a roughly linear increase of the front deformations with increasing fracture toughness contrast. For brittle materials (i.e. no process zone size), the Fourier transform of the quasi-static front deformations δa is given by, see [9],

$$\widehat{\delta a}(k) = -\frac{1}{|k|}\frac{\widehat{\delta G_c(k)}}{G_c^0} \tag{S6}$$

with k the wavenumber and $\hat{\cdot}$ indicates a Fourier transform. Eq. (S6) predicts a linear dependency of the front

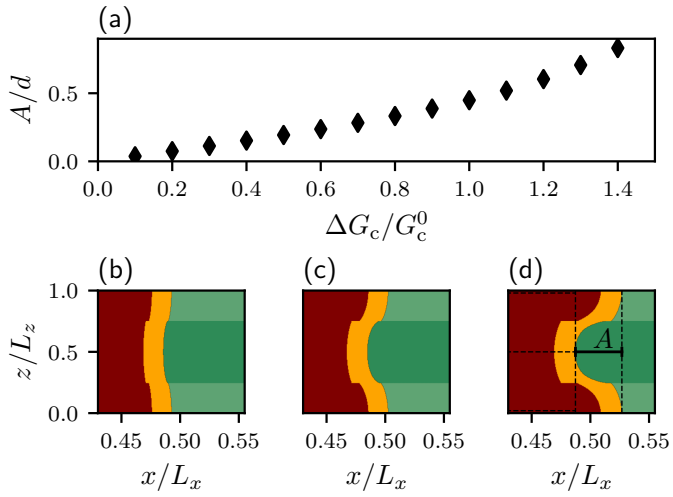

FIG. S3. (a) Scaling of the amplitude A of the front deformations with the toughness contrast $\Delta G_c/G_c^0$. (b)-(c)-(d): snapshots of the crack front deformation for respectively $\Delta G_c/G_c^0 = 0.3, 0.7, 1.2$. The crack is in brown, the process zone in orange, the strong toughness in dark green and the weak one in light green. The crack velocity in these simulations is $v_c = 0.5c_R$.

amplitude on the toughness contrast, which is consistent with our observations. For large contrasts, the observations deviate from the predictions, which is expected as second-order effects start being relevant.

Effect of dynamics on crack front deformations

We now wish to assess the influence of dynamics on the crack front deformations. We will consider a permanent regime, i.e. a crack that has been propagating at a constant velocity for an infinite amount of time. An expression for the perturbation of the dynamic stress intensity factor for a small deviation from straightness of a crack is provided by [10]. The general structure of the equation relates the perturbed stress intensity factor to the original stress intensity factor and a convolution of the front deformation with a function P, see Eq. (8.10) in [10]. For a mode I crack, its perturbed stress intensity factor K_I writes as Eq. (S7). K_I^0 is the stress intensity factor in the unperturbed configuration, and PV denotes a Cauchy principal value. $P(z,t)$ is a kernel whose expression in the wavenumber-frequency domain $(z \to k), (t \to \theta)$ is given by [8, 11]. We consider only the permanent regime for which there is no time dependency $(\theta = 0)$ and in this case $P(z,t)$ reduces to $D_I(v)|k|/2$ with $D_I(v)$ given by Eq. (S8). It corresponds to the dynamic stiffening term associated with mode I solicitation. We show the function $D_I(v)$ in Fig. S4. It tends towards 1 for the quasi-static case $v_c = 0$ and towards 0 for cracks approaching the limiting propagation velocity, the Rayleigh wave speed c_R.

$$K_I(z,t) = K_I^0(z) + \delta K_I(z,t) = K_I^0(z) + \frac{\delta K_I^0}{\partial a}(z)\delta a(z,t) - \mathrm{PV}\int_{-\infty}^{+\infty} P(z,t)K_I^0(z')\left[\delta a(z,t) - \delta a(z',t)\right]dz' \tag{S7}$$

$$D_I(v_c) = 1/\left(\frac{2}{\sqrt{1-(v_c/c_R)^2}} - \frac{1}{\sqrt{1-(v_c/c_d)^2}} - (v_c/c_R)^2\int_{c_s}^{c_d}\phi(v)dv\right) \tag{S8}$$

$$\phi(v) = \sqrt{\frac{2}{\pi\left[(v/c_R)^2 - (v_c/c_R)^2\right]}}\arctan\left(\frac{4\sqrt{1-(v/c_d)^2}\sqrt{(v/c_s)^2-1}}{(2-(v/c_s)^2)^2}\right) \tag{S9}$$

Dynamic Cohesive Line Tension Model

In order to derive a dynamic cohesive line tension model, one can build on the derivation for the quasi-static cohesive line tension model of Lebihain et al. [9] to compute the expression of the stress intensity factor k of the deformed front $\mathcal{F}^*$ that is generated at a point $z = z_0$ by a pair of unitary forces that are applied at a given distance x behind the crack front at a point $z = z_1$, see Eq. (7) in [9]. In the permanent dynamic regime, it writes

$$k\left(\mathcal{F}^*; z_0, z_1, x, v_c\right) = k\left(\mathcal{F}; z_0, z_1, x, v_c\right) + D_I(v_c)\int_{-\infty}^{+\infty} k\left(\mathcal{F}; z; z_1, x, v_c\right)\frac{\delta a(z) - \delta a(z_1)}{(z-z_1)^2}dz \tag{S10}$$

where $k\left(\mathcal{F}; z_0, z_1, x, v_c = 0\right)$ is known analytically for the semi-infinite coplanar crack with a straight crack

front $\mathcal{F}$, see [9] for more details on the derivation of the crack face weight functions.

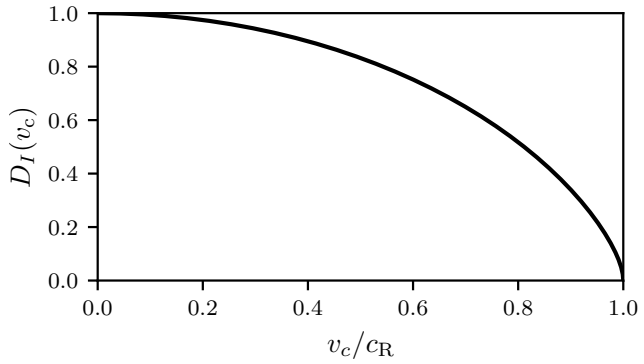

FIG. S4. Dynamic pre-factor $D_I(v_c)$ from Eq. (S8) as a function of the propagation velocity v_c/c_r.

The derivation of the dynamic cohesive line tension model follows then the one presented in [9] for the crack face weight functions and the cohesive stress intensity factor, with the difference that the process zone to be considered is the instantaneous cohesive zone size ω_v instead of the rest one ω_0, and the pre-factor $D_I(v_c)$ multiplying the terms. The complete prediction for the deformation of a front in the dynamic regime due to both heterogeneities of strength and process zone thus corresponds to Eq. (53) in [9] with the two changes mentioned above, which result in Eq. (2). Note that as $D_I(v_c = 0) = 1$, we recover the formulae given by [9] for the quasi-static front deformation in presence of a process zone. For cracks propagating at the limiting velocity, we have $D_I(v_c = c_R) = 0$, resulting in theoretically undeformable crack front in this limit (in the hypothesis of co-planar crack propagation). In practice, fast cracks will often trigger out-of-plane damage and instabilities before reaching the limiting velocity.

For completeness, we recall here the expression for $\hat{\mathcal{A}}$ and $\hat{\Sigma}$ and $\hat{\Omega}$. Note that these expressions slightly differ from the one given by [9] as we consider here the dynamic process zone size ω_v and not the static one ω_0.

$$\begin{cases} \hat{\mathcal{A}}\left(|k|\omega_v\right) & = -\dfrac{1}{C_w}\int_0^{+\infty}\dfrac{f'_w\left(u\right)}{u^{1/2}}\left(1-e^{-|k|\omega_v u}\right)du \\ \hat{\Sigma}\left(|k|\omega_v\right) & = \dfrac{1}{C_w}\int_0^{+\infty}\dfrac{f_w\left(u\right)}{u^{1/2}}e^{-|k|\omega_v u}du \\ \hat{\Omega}\left(|k|\omega_v\right) & = -\dfrac{2}{C_w}\int_0^{+\infty}f'_w\left(u\right)u^{1/2}e^{-|k|\omega_v u}du \end{cases} \tag{S11}$$

with $C_w = \int_0^{+\infty} f_w\left(u\right) u^{-1/2} du$ and $f_w(x/\omega)$ the shape function that relates to the nature of the weakening. For the linear traction separation law considered in this work there is no analytical expression for the shape function as a function of the distance, but it can be computed numerically, see [9] Appendix C.4. for details. $\hat{\mathcal{A}}$ and $\hat{\Sigma}$ and $\hat{\Omega}$ for other cohesive laws such as linear distance weakening, Dugdale-Barenblatt distance weakening [12, 13] and exponential distance weakening are also provided in Appendix C of [9].

[1] T. Roch, F. Barras, P. H. Geubelle, and J.-F. Molinari, J. Open Source Softw. **7**, 3724 (2022).
[2] P. H. Geubelle and J. R. Rice, J. Mech. Phys. Solids **43**, 1791 (1995).
[3] J. W. Morrissey and P. H. Geubelle, Int. J. Numer. Methods Eng. **40**, 1181 (1997).
[4] M. S. Breitenfeld and P. H. Geubelle, Int. J. Fract. **93**, 13 (1998).
[5] T. Roch, M. Lebihain, and J.-F. Molinari, cRacklet simulations for "dynamic crack front deformations in cohesive materials".
[6] J. W. Morrissey and J. R. Rice, J. Mech. Phys. Solids **46**, 467 (1998).
[7] F. Fekak, F. Barras, A. Dubois, D. Spielmann, D. Bonamy, P. H. Geubelle, and J. F. Molinari, J. Mech. Phys. Solids **135**, 103806 (2020).
[8] S. Ramanathan and D. S. Fisher, Phys. Rev. Lett. **79**, 877 (1997).
[9] M. Lebihain, T. Roch, and J.-F. Molinari, J. Mech. Phys. Solids **168**, 105025 (2022).
[10] J. R. Willis and A. B. Movchan, J. Mech. Phys. Solids **43**, 319 (1995).
[11] J. W. Morrissey and J. R. Rice, J. Mech. Phys. Solids **48**, 1229 (2000).
[12] D. S. Dugdale, J. Mech. Phys. Solids **8**, 100 (1960).
[13] G. I. Barenblatt, in *Adv. Appl. Mech.*, Vol. 7, edited by H. L. Dryden, T. von Kármán, G. Kuerti, F. H. van den Dungen, and L. Howarth (Elsevier, 1962) pp. 55–129.